European Radiology (2023) 33:6817–6827
https://doi.org/10.1007/s00330-023-09693-y

European Radiology
ESR EUROPEAN SOCIETY OF RADIOLOGY

IMAGING INFORMATICS AND ARTIFICIAL INTELLIGENCE

Deep learning HASTE sequence compared with T2-weighted BLADE sequence for liver MRI at 3 Tesla: a qualitative and quantitative prospective study

Pierre Wary[1] · Gabriela Hossu[2,3] · Khalid Ambarki[4] · Dominik Nickel[5] · Simon Arberet[6] · Julien Oster[2,3] · Xavier Orry[1] · Valérie Laurent[1,3]

Received: 21 August 2022 / Revised: 26 February 2023 / Accepted: 11 March 2023 / Published online: 16 May 2023

Abstract

Objectives To qualitatively and quantitatively compare a single breath-hold fast half-Fourier single-shot turbo spin echo sequence with deep learning reconstruction (DL HASTE) with T2-weighted BLADE sequence for liver MRI at 3 T.

Methods From December 2020 to January 2021, patients with liver MRI were prospectively included. For qualitative analysis, sequence quality, presence of artifacts, conspicuity, and presumed nature of the smallest lesion were assessed using the chi-squared and McNemar tests. For quantitative analysis, number of liver lesions, size of the smallest lesion, signal-to-noise ratio (SNR), and contrast-to-noise ratio (CNR) in both sequences were assessed using the paired Wilcoxon signed-rank test. Intraclass correlation coefficients (ICCs) and kappa coefficients were used to assess agreement between the two readers.

Results One hundred and twelve patients were evaluated. Overall image quality ($p = .006$), artifacts ($p < .001$), and conspicuity of the smallest lesion ($p = .001$) were significantly better for the DL HASTE sequence than for the T2-weighted BLADE sequence. Significantly more liver lesions were detected with the DL HASTE sequence (356 lesions) than with the T2-weighted BLADE sequence (320 lesions; $p < .001$). CNR was significantly higher for the DL HASTE sequence ($p < .001$). SNR was higher for the T2-weighted BLADE sequence ($p < .001$). Interreader agreement was moderate to excellent depending on the sequence. Of the 41 supernumerary lesions visible only on the DL HASTE sequence, 38 (93%) were true-positives.

Conclusion The DL HASTE sequence can be used to improve image quality and contrast and reduces artifacts, allowing the detection of more liver lesions than with the T2-weighted BLADE sequence.

Clinical relevance statement The DL HASTE sequence is superior to the T2-weighted BLADE sequence for the detection of focal liver lesions and can be used in daily practice as a standard sequence.

Key Points

- *The half-Fourier acquisition single-shot turbo spin echo sequence with deep learning reconstruction (DL HASTE sequence) has better overall image quality, reduced artifacts (particularly motion artifacts), and improved contrast, allowing the detection of more liver lesions than with the T2-weighted BLADE sequence.*
- *The acquisition time of the DL HASTE sequence is at least eight times faster (21 s) than that of the T2-weighted BLADE sequence (3–5 min).*
- *The DL HASTE sequence could replace the conventional T2-weighted BLADE sequence to meet the growing indication for hepatic MRI in clinical practice, given its diagnostic and time-saving performance.*

Keywords Deep learning · Magnetic resonance imaging · Liver · Diagnostic imaging · Neural networks, computer

✉ Pierre Wary
P.WARY@chru-nancy.fr

[1] Department of Adult Radiology, CHRU de Nancy, 5 Rue du Morvan, 54500 Vandoeuvre-lès-Nancy, France

[2] Clinical Investigation Center Technological Innovation of Nancy, Inserm, CHRU de Nancy, Vandoeuvre-lès-Nancy, France

[3] Adaptive Diagnostic and Interventional Imaging, Inserm, CHRU de Nancy, Vandoeuvre-lès-Nancy, France

[4] Siemens Healthcare, Siemens Healthcare SAS, Saint Denis, France

[5] Siemens Healthcare GmbH, MR Application Predevelopment, Erlangen, Germany

[6] Siemens Healthineers, Digital Technology & Innovation, Princeton, NJ, USA

Abbreviations

AIMANT	Optimization of the acquisition sequence to improve the quality and comfort of magnetic resonance imaging exam
CNR	Contrast-to-noise ratio
DL HASTE	Half-Fourier acquisition single-shot turbo spin echo using deep learning reconstruction
FA	Flip angle
HASTE	Half-Fourier acquisition single-shot turbo spin echo
ICC	Intraclass correlation coefficient
SAR	Specific absorption rate
SNR	Signal-to-noise ratio
TE	Echo time
TSE	Turbo spin echo

Introduction

In hepatic MRI, T2-weighted imaging facilitates the detection and characterization of hepatic lesions [1–4]. However, its long acquisition time causes numerous artifacts from the patient's respiratory movements. The development of turbo spin echo (TSE) sequences with respiratory triggering or the use of free-breathing in combination with parallel imaging initially enabled reduced acquisition times and artifacts [5–10]. MR manufacturers have developed sequences using k-space sampling strategies to further reduce motion artifacts (PROPELLER at General Electric, BLADE at Siemens, MultiVane at Philips) [11–16]. Although the image quality has been significantly improved, the acquisition time is still too long in view of the increasing indications for MRI examinations [17, 18].

The half-Fourier acquisition single-shot turbo spin echo (HASTE) sequence is a single-shot sequence that is used to acquire all the raw imaging data needed for a slice in a few hundred milliseconds using a single echo train following a 90° excitation pulse. Thus, it is robust to motion, and related artifacts are therefore significantly reduced [19, 20]. Compared to a conventional T2-weighted sequence, a HASTE sequence uses a partial Fourier acquisition to ensure the desired echo time (TE) for center k-space lines, and uses longer echo trains.

Depending on the extent of partial Fourier sampling and the duration of the echo train, the image contrast can be affected. The T2 decay during the acquisition of an echo train leads to high T2 weighting at higher frequencies, and the resulting images suffer from a significant degradation of the signal-to-noise ratio (SNR) due to the weak intensity of the late echo signals [21]. The spatial resolution is also reduced with the presence of blurring in the direction of phase encoding [19]. To improve the image quality of the HASTE sequence and make the image contrast more comparable to that of conventional TSE imaging, a shorter echo train, less aggressive partial Fourier imaging, and a higher SNR have been used.

One avenue of research could be the use of a deep learning–based reconstruction associated with the HASTE sequence (DL HASTE), such as the sequence recently developed by one vendor, which would allow for higher acceleration and image acquisition with a better SNR. Moreover, it could allow a reduction in the echo train length due to an additional separate acquisition of the calibration data.

In previous retrospective studies, the DL HASTE sequence on abdominal MRI at 1.5 T has been compared with the T2-weighted BLADE sequence [22, 23] and the T2 TSE sequence [24]. Herrmann J et al studied the impact of flip angle variation on the image quality and diagnostic confidence and then retrospectively compared the DL HASTE sequence and T2-weighted BLADE sequence for a small number of patients for liver MRI at 3 T [25]. More recently, Ginocchio et al compared the DL HASTE sequence for liver MRI at 3 T with the conventional T2 TSE sequence [26].

To our knowledge, our study is the first to prospectively compare, qualitatively and quantitatively, the DL HASTE and T2-weighted BLADE sequences for liver MRI at 3 T. In addition, we quantitatively compare the two sequences by measuring the signal-to-noise ratio and the contrast-to-noise ratio, which has not yet been performed in other studies at 3 T.

The objective of this study is to qualitatively and quantitatively compare the DL HASTE sequence with the conventional T2-weighted BLADE for 3-T liver MRI acquisitions. We hypothesize that the DL HASTE sequence is neither qualitatively nor quantitatively inferior to the conventional T2-weighted BLADE sequence and has a much shorter acquisition time.

Methods

Study population

The AIMANT (optimization of the acquisition sequence to improve the quality and comfort of magnetic resonance imaging exam, NCT04645628) study was conducted in compliance with the Declaration of Helsinki and was approved by the institution's Ethics Committee (number 2020-063B).

Consecutive adult patients referred in our institution for a clinically indicated liver MRI between December 2020 and January 2021 were included in this prospective, monocenter study. Missing patient data and incomplete MRI datasets were considered exclusion criteria.

All participants provided written informed consent.

MRI acquisitions

All MR examinations were performed using the same 3-T clinical MR scanner (MAGNETOM Skyra; Siemens

Healthcare), using a body array coil with 18 channels and a spine array coil with 32 channels, with the patient in the dorsal decubitus position. For each patient, the MR imaging protocol included a fat-suppressed T2-weighted BLADE sequence with navigator-triggered prospective acquisition correction (PACE) in the axial plane and a fat-suppressed DL HASTE sequence with a single breath-hold in the axial orientation.

The acquisition parameters of both sequences are detailed in Table 1.

The modifications applied to the prototypical DL HASTE sequence compared to the conventional HASTE sequence are aimed at shortening the echo train duration, reducing the specific absorption rate (SAR), reducing T2-blurring, and shortening the overall acquisition time. To shorten the duration of the echo train, a separate acquisition of the reference data for the estimation of coil sensitivity maps was performed. This was realized by a second echo train following the acquisition of the imaging data. The SAR was thereby reduced by having fewer refocusing pulses in the echo train and the use of a higher acceleration factor compared with that of the conventional sequence. Furthermore, a variable flip angle evolution for the refocusing pulses was used to reduce the SAR and delay the T2 relaxation. The evolution was determined by the initial flip angle (130°), the minimal flip angle (100°), the flip angle at the k-space center (120°), and the final flip angle (140°) [27]. The effective echo time (TE) was 99 ms, the apparent TE due to the delayed T2 decay was 79 ms, and the repetition time (TR) was set to 595 ms. Compared to the conventional HASTE sequence, the slice increment between sequentially acquired slices was set to 4 to mitigate signal attenuation due to crosstalk and magnetization transfer at such a small TR.

Other sequences analyzed in the complementary analysis included diffusion-weighted imaging (*b* values of 50, 500, and 800 s/mm^2) performed in free-breathing using a simultaneous multislice echoplanar imaging (SMS-EPI) system. A T1-weighted VIBE sequence with fat suppression using spectral attenuated recovery in one breath-hold was also analyzed. After a precontrast acquisition, a standard dose (0.2 mL/kg) of gadoxetic acid (Clariscan; GE Healthcare) was intravenously injected at a rate of 2 mL/s by using a power injector (OptiStar Elite; Guerbet) followed by a 20 mL saline flush. Arterial phase images were acquired 20 s after contrast administration, and portal venous phase and delayed phase images were obtained 80 s and 3 min after contrast administration, respectively. Detailed information about these sequences is summarized in Supplemental Table 1.

Table 1 Acquisition parameters of the T2-weighted BLADE and DL HASTE sequences on 3-T liver MRI

Parameters	T2-weighted BLADE	DL HASTE
Orientation	Axial	Axial
Respiration	Navigator-triggering	Single breath-hold
TE/TR, ms	105/ > 2000	99/595
Slice thickness, mm	5.5	5.5
FA, degrees	180	130–100-120–140
Voxel size, mm^3	1.1 × 1.1 × 5.5	1.1 × 1.1 × 5.5
Matrix size	320 × 320	384 × 300
Acceleration factor	2	3
Acquisition time, min:s	3–5	0:21

Abbreviations: *DL HASTE*, half-Fourier acquisition single-shot turbo spin echo using deep learning; *TE*, echo time; *TR*, repetition time; *FA*, flip angle

Image reconstruction with deep learning HASTE

Image reconstruction of the DL HASTE sequence is achieve by using an unrolled iterative reconstruction network, where a gradient step that improves the data consistency is followed by a regularization step. This architecture shares some similarities with the variational network as introduced previously [28]. The network uses coil sensitivity maps that have been precomputed from a separate reference scan, k-space data, and bias-field correction.

This network uses two types of iterations; each of them has data consistency and trainable (Nesterov-type) extrapolation steps [29]. The first 22 iterations contain a trainable extrapolation and a data consistency step but no image regularization. The goal is to first minimize the data consistency and only focus on parallel imaging reconstruction. In the next 12 iterations, image regularization via a residual dense U-Net [30] is added after each data consistency step [24] to enhance the image quality.

Training data were acquired on volunteers using the conventional HASTE sequence. The imaging protocols were based on the vendor-supplied HASTE protocols for the abdomen in the axial and coronal orientations. The acquisitions were performed with an acceleration factor of 2, and the ground truth images required for the supervised training procedure were reconstructed using an unregularized SENSE reconstruction with the same estimated coil sensitivity maps as those used in the network reconstruction. As input to the network in the training phase, the k-space was then retrospectively downsampled to an acceleration factor of 4. In total, more than 10,000 slices were acquired for training. Compared to the protocols provided with the scanner, acquisition parameters were varied in the following ranges: TE from 81 to 200 ms, TR from 550 to 3800 ms, base resolution from 256 to 384, phase resolution from 70 to 95%, and phase oversampling from 0 to 50%. Acquisitions varied between unprepared, spectrally fat-suppressed, and inversion recovery prepared image contrasts. The acquisitions were performed on various clinical

1.5-T and 3-T scanners (MAGNETOM scanners, Siemens Healthcare) with a relative ratio of approximately 1:2.

Analysis of MRI images

MRI images were analyzed on a Picture Archiving and Communication System (PACS) viewing station (DirectView, version 12.2.2.1025, Carestream Health Inc.) by P.W., a radiology resident, and V.L., a radiologist with 15 years of experience in abdominal imaging. Each reviewer was blinded to the patient identification, clinical information, and possible biopsy results. Each sequence was assessed separately and without knowledge of the other sequences. Qualitative analysis and lesion identification of the T2-weighted BLADE and DL HASTE sequences were performed in two separate sessions, 1 month apart, to avoid possible recall bias. This review was performed for all participants for P.W. and for thirty randomly selected participants for V.L.

P.W. performed a third session 1 month later on all participants for the measurement of signal-to-noise ratio (SNR) and contrast-to-noise ratio (CNR) in a joint unblinded analysis of the two sequences to allow for reproducibility of measurements and to avoid potential measurement bias.

P.W. performed a fourth session on all participants in a joint non-blinded complementary analysis with all liver MRI sequences to define true-positive and false-positive lesions.

Qualitative analysis

Qualitative analysis was performed subjectively with assessment of the overall quality of the sequence rated on a scale of 1 to 5 (1 = "mediocre," 2 = "poor," 3 = "moderate," 4 = "good," 5 = "excellent") and presence of artifacts on a scale of 0 to 2 (0 = "no artifact," 1 = "present but not interfering with interpretation," 2 = "present and interfering with interpretation"). The reviewer then had to identify the smallest hepatic lesion larger than 5 mm and specify its conspicuity on a scale of 1 to 5 (1 = "mediocre," 2 = "poor," 3 = "moderate," 4 = "good," 5 = "excellent") as well as its presumed nature on a scale of 0 to 3 (0 = "difficult to ascertain," 1 = "liquid," 2 = "solid," 3 = "mixed") and its location according to the Couinaud classification of liver segments [31].

Quantitative analysis

Identification of lesions

For each sequence, the total number of focal hepatic lesions (> 5 mm) and the size of the smallest visible focal hepatic lesion were recorded. Histopathologic confirmation was not obtained for lesions identified by investigators as focal hepatic lesions.

Signal-to-noise ratio and contrast-to-noise ratio measurements

To characterize the hepatic signal, a circular 20-mm-diameter region of interest (ROI) was placed in a healthy part of the right hepatic lobe while excluding hepatic vessels, lesions, any artifacts (repetition, metallic, etc.), and sudden signal changes as much as possible.

For the contrast measurement, maximum-sized circular ROIs were placed inside the two largest hepatic lesions identified by the investigator. The ROIs had to be placed within lesion edges and had to include all the components of the lesion if it was heterogeneous. For each ROI placed on a lesion, an identically sized ROI was placed in adjacent healthy parenchyma while excluding hepatic vessels, other lesions, any artifacts, and sudden signal changes as much as possible.

Each ROI was reproduced identically in terms of size and placement on the other investigated MRI sequence of the same patient in a joint unblinded analysis of the two sequences. The ROIs were replicated on the other sequence on synchronized slices, automatically or with manual adjustment, between the two sequences to allow the reproducibility of measurements.

In parallel imaging, noise is not evenly distributed across the image [21, 32]. Consequently, it cannot be measured globally and be accurately estimated by a measurement in a homogeneous region outside of the object of interest. Although an accurate measurement of noise across the entire image is impossible, a local estimate of the noise can be obtained. Therefore, in our study, we measured noise locally in a region close to the target signal measurement site, as suggested by Heverhagen [33].

The SNR was calculated according to the following formula:

$$\mathrm{SNR} = \frac{\mathrm{SI}_{\mathrm{liver}}}{\mathrm{N}_{\mathrm{liver}}}$$

where $\mathrm{SI}_{\mathrm{liver}}$ is the mean of the liver signal and $\mathrm{N}_{\mathrm{liver}}$ is the standard deviation of the liver signal.

The CNR was calculated according to the following formula:

$$\mathrm{CNR} = \frac{(\mathrm{SI}_{\mathrm{lesion}} - \mathrm{SI}_{\mathrm{adja}})}{\mathrm{N}_{\mathrm{adja}}}$$

where $\mathrm{SI}_{\mathrm{lesion}}$ is the mean of the signal from the hepatic lesion, $\mathrm{SI}_{\mathrm{adja}}$ is the mean of the signal from the adjacent

healthy liver, and N_{adja} is the standard deviation of the signal from the adjacent healthy liver.

Complementary analysis

P.W. performed a complementary analysis on images of participants who had supernumerary liver lesions visible only on the DL HASTE sequence and not visible on the T2-weighted BLADE sequence or visible on the T2-weighted BLADE sequence and not visible on the DL HASTE sequence.

For each of these supernumerary lesions, their size and location according to the Couinaud classification were recorded. A joint nonblind analysis with the five other hepatic MRI sequences (diffusion-weighted imaging and T1-weighted VIBE: precontrast, arterial phase, venous phase, and delayed phase) allowed us to define whether the lesion was visible on these sequences.

The lesion is defined as visible when it appears in a hypersignal at any *b* value on diffusion-weighted imaging or when it appears in a hypersignal or hyposignal on T1 VIBE precontrast and/or T1 VIBE postcontrast sequences.

Statistical analysis

Continuous variables are expressed as the median ± interquartile range (IQR), and categorical variables are expressed as frequencies (percentages). The normality of the distribution was tested by using the Shapiro-Wilk test.

A paired Wilcoxon signed-rank test with continuity correction was used to compare the number of visible lesions, their sizes, and the CNR and SNR between the two sequences. The chi-square test was used to compare the quality, presence of artifacts, and conspicuity of the smallest lesion between the two sequences. McNemar's test was used to compare the presumed nature of the smallest lesion between the two sequences (dichotomized into two groups: presumed nature judged as "difficult to ascertain" versus "liquid" or "solid" or "mixed").

A multivariate logistic analysis was performed to determine a potential relationship between the quality of the examination (dichotomized into two groups: quality assessed as "good" or "excellent" versus "moderate" or "poor" or "mediocre") and the following three explanatory variables: age, BMI, and presence of ascites.

A p value < 0.05 was considered to indicate a statistically significant difference.

Intraclass correlation coefficients (two-way random effects, absolute agreement) (ICCs) were used to assess the interreader agreement for quantitative variables such as the total number of focal liver lesions detected and the size of the smallest visible focal liver lesion. The weighted kappa (κ_w) values were used for the agreement of ordinal qualitative data such as the overall quality, presence of artifact, and conspicuity of the smallest lesion, and Cohen's kappa (κ) was used for the nominal qualitative data such as the presumed nature of the smallest lesion and its location.

ICCs or κ coefficients between 0.81 and 1.00 indicate an excellent agreement; those between 0.61 and 0.80 indicate a strong agreement; those between 0.41 and 0.60 indicate a moderate agreement; those between 0.21 and 0.40 indicate a moderate agreement; and those between 0.00 and 0.20 indicate a poor agreement.

For complementary analyses, the size, location, and number of true-positives and false-positives of supernumerary lesions were calculated. A true-positive is defined as a lesion visible only on the DL HASTE or T2-weighted BLADE sequence and visible on at least one of the other five liver MRI sequences. A false-positive is defined as a lesion visible only on the DL HASTE or T2-weighted BLADE sequence and not visible on the five other sequences.

Statistical analysis was performed by G.H. using R software, version 4.0.3, R Project for Statistical Computing, including its CBCGrps library [34].

Results

Patient characteristics

We enrolled 114 patients in the AIMANT study. Of these, two patients were excluded because of missing MRI data. The data from a total of 112 participants were analyzed (Fig. 1). The mean age ± standard deviation was 62.5 years ± 13.9; 75 participants (67%) were men; the mean body mass index ± standard deviation was 27.9 kg/m^2 ± 5.9. Table 2 summarizes the baseline characteristics of the participants.

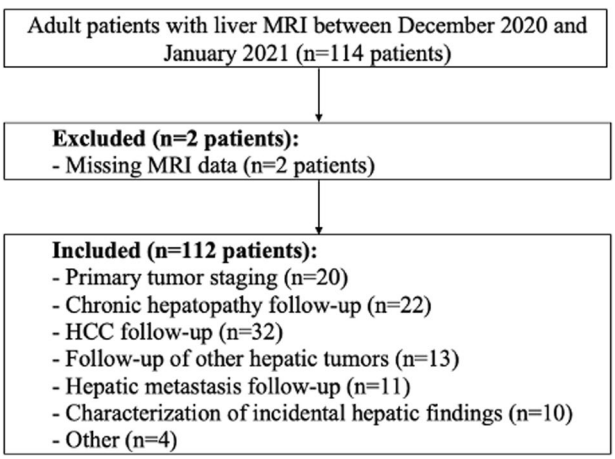

Fig. 1 Flowchart of patients through the AIMANT study. Abbreviations: HCC, hepatocellular carcinoma

Table 2 Baseline characteristics of the study population

Characteristics	Value
Study population, *n*	112
Gender, *n* (%)	
Male	75 (67%)
Female	37 (33%)
Age, mean ± SD (range), year	62.5 ± 13.9 (21–86)
BMI, mean ± SD (range), kg/m^2	27.9 ± 5.9 (16.4–48.3)
Ascites, *n*	12 (11%)
Indication for MRI, *n* (%)	Primary tumor staging, 20 (18%)
	Chronic hepatopathy follow-up, 22 (20%)
	HCC follow-up, 32 (28%)
	Follow-up of other hepatic tumors, 13 (12%)
	Hepatic metastasis follow-up, 11 (10%)
	Characterization of incidental hepatic findings, 10 (9%)
	Other, 4 (3%)

Abbreviations: *SD*, standard deviation; *BMI*, body mass index; *HCC*, hepatocellular carcinoma

Qualitative analysis

The results of the qualitative analysis are summarized in Table 3.

The quality of the examination was significantly higher with the DL HASTE sequence; 69% (77 cases) of the exams were assessed as having good to excellent image quality (≥ 4) using the DL HASTE sequence versus 44% (49 cases) with the T2-weighted BLADE sequence ($p = 0.006$; Fig. 2).

The presence of artifacts was significantly lower for the DL HASTE sequence than for the T2-weighted BLADE sequence ($p < 0.001$), with only 9% (10 cases) of the examinations assessed with artifacts interfering with interpretation for the DL HASTE sequence against 18% (20 cases) for the T2-weighted BLADE sequence (Fig. 2).

The conspicuity of the smallest focal hepatic lesion was significantly better for the DL HASTE sequence, with 71% of the lesions assessed with good to excellent conspicuity (≥ 4) versus 39% with the T2-weighted BLADE sequence ($p = 0.001$; Fig. 3).

The presence of ascites was identified as a potential explanatory variable, although no significant difference was observed between the two sequences in this subset of patients ($p = 0.096$).

Quantitative analysis

The results of the quantitative analysis are summarized in Table 4.

Significantly more lesions were identified using the DL HASTE sequence (median, 1; IQR, 0–4) than the T2-weighted BLADE sequence (median, 1; IQR, 0–3.25; $p < 0.001$). We identified 356 lesions on the DL HASTE sequence versus 320 lesions on the T2-weighted BLADE sequence (Fig. 4).

The SNR values of the liver parenchyma were significantly better for the T2-weighted BLADE sequence (median, 10.28; IQR, 8.1–12.3) than for the DL HASTE sequence (median,

Table 3 Results of the qualitative analysis of the DL HASTE and T2-weighted BLADE sequences

Qualitative variables	DL HASTE	T2-weighted BLADE	*p* value
Quality, scores, *n* (%)			.006
1–2	11 (10)	19 (16)	
3	24 (21)	44 (40)	
4–5	77 (69)	49 (44)	
Artifacts, scores, *n* (%)			< .001
0	89 (79)	58 (52)	
1	13 (12)	34 (30)	
2	10 (9)	20 (18)	
Conspicuity of the smallest lesion, scores, *n* (%)			.001
1–2	11 (14)	18 (23)	
3	12 (15)	30 (38)	
4–5	56 (71)	31 (39)	
Presumptive nature of the smallest lesion, scores, *n* (%)			.07
0	9 (11)	15 (19)	
1	50 (63)	47 (59)	
2	17 (22)	14 (18)	
3	3 (4)	3 (4)	

Abbreviations: *DL HASTE*, half-Fourier acquisition single-shot turbo spin echo using deep learning

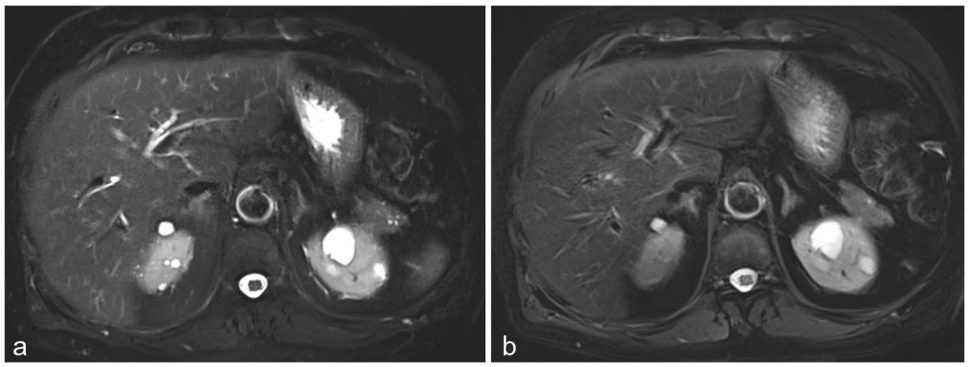

Fig. 2 Characterization of focal liver lesions in a 68-year-old male. The DL HASTE axial image (**a**) shows better overall image quality and fewer motion artifacts than the T2-weighted BLADE axial image (**b**)

9.41; IQR, 7.44–11.05; $p < 0.001$). The CNR values of liver lesions were, however, significantly better for the HASTE DL sequence (median, 17.11; IQR, 7.86–31.67) than for the T2-weighted BLADE sequence (median, 12.10; IQR, 6.13–20; $p < 0.001$; Fig. 5).

Interreader agreement

The interreader agreement between the two radiologists for the DL HASTE sequence was excellent for the total number of focal liver lesions detected (ICC, 0.986) and the size of the smallest visible liver lesion (ICC, 0.997). It was strong to excellent for the overall quality (κ_w, 0.820), presence of artifacts (κ_w, 0.789), conspicuity of the smallest lesion (κ_w, 0.836), presumed nature (κ, 0.65), and location (κ, 0.94).

For the T2-weighted BLADE sequence, the interreader agreement was excellent for the total number of focal liver lesions detected (ICC, 0.974) and the size of the smallest visible liver lesion (ICC, 0.998). It was moderate to excellent for the overall quality (κ_w, 0.788), presence of artifacts (κ_w, 0.712), conspicuity of the smallest lesion (κ_w, 0.733), presumed nature (κ, 0.58), and location (κ, 0.94).

Complementary analysis

The results of the complementary analysis are summarized in Table 5.

Of the 41 supernumerary lesions visible only on the DL HASTE sequence, 38 (93%) were true-positives that were also visible on the other MRI sequences, and 3 (7%) were false-positives. The true-positives were located mainly on segments 2 (11 lesions; 27%) and 8 (9 lesions; 22%).

All 5 supernumerary lesions visible only on the T2 BLADE-weighted sequence were true-positives.

Discussion

In this study, we assessed the qualitative and quantitative performances of the DL HASTE sequence compared to the conventional T2-weighted BLADE sequence for liver 3-T MRI. It was found that the image quality significantly improved, the presence of artifacts was reduced, the conspicuity of small lesions was improved, and a larger number of hepatic lesions could be detected using the DL HASTE sequence compared to using the T2-weighted BLADE sequence.

One possible explanation for these results is the fast speed of acquisition. Indeed, all slices of the sequence were obtained in 21 s in a single breath-hold.

This allowed us to obtain a robust and reproducible sequence with fewer artifacts—particularly motion artifacts [19, 20, 35]. Moreover, given the high number of focal hepatic lesions in a T2 hypersignal, the strong T2 weighting of the HASTE sequence linked to the filling of the majority

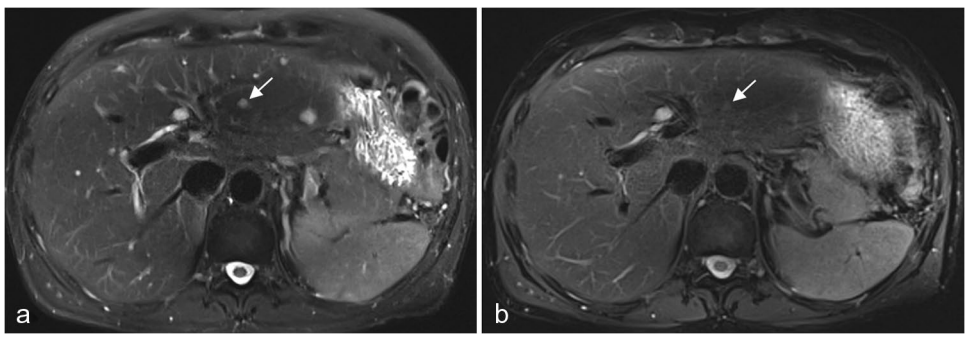

Fig. 3 Characterization of focal liver lesions in a 59-year-old male followed for a renal cell carcinoma. The DL HASTE axial image (**a**) shows better conspicuity for a small 5-mm focal liver lesion (arrow) than the T2-weighted BLADE axial image (**b**). Other focal hepatic lesions, particularly those of the left liver, are also better visualized on the DL HASTE image

Table 4 Results of the quantitative analysis of the DL HASTE and T2-weighted BLADE sequences

Quantitative variables	DL HASTE	T2-weighted BLADE	*p* value
Number of lesions			< .001
Median	1	1	
IQR	0;4	0;3.25	
Total, *n*	356	320	
Size of the smallest lesion, mm			0.5
Median	7	8	
IQR	6;14.5	6;15	
SNR			< .001
Median	9.41	10.28	
IQR	7.44;11.05	8.1;12.3	
CNR			< .001
Median	17.11	12.10	
IQR	7.86;31.67	6.13;20	

Abbreviations: *DL HASTE*, half-Fourier acquisition single-shot turbo spin echo using deep learning; *IQR*, interquartile range; *SNR*, signal-to-noise ratio; *CNR*, contrast-to-noise ratio

of k-space with long-TE echoes [19, 20, 35] enabled excellent contrast to be obtained, thus resulting in greater conspicuity and detection of small lesions.

A better CNR was obtained using the DL HASTE sequence than the T2-weighted BLADE sequence, whereas a better SNR was obtained using the T2-weighted BLADE sequence. An increase in image noise and image blurring in single-shot sequences [20, 35] due to an important difference in signal intensity between two lines in the k-space during a long echo train may represent a possible explanation for the decrease in SNR. Another possible explanation could stem from training of the neural network on a relatively small number of patient data, inducing an insufficient increase in signal intensity on the late echoes. In addition, fat saturation of the DL HASTE sequence induces a decrease in overall signal intensity [19, 20]. Although signal intensity decreases globally in the image, the contrast-to-noise ratio is better with the DL HASTE sequence, which is a crucial element for hepatic lesion detection.

Of the 38 true-positives of supernumerary lesions visible only on the DL HASTE sequence, the great majority seemed to be explained by the presence of artifacts, notably motion artifacts on the T2-weighted BLADE sequence, which did not allow detection of these lesions. Moreover, this hypothesis seems to be supported by the fact that these lesions were preferentially localized in liver segments 2 and 8, which are subject to more artifacts, particularly those related to cardiac movements. Of the 3 false-positives with the DL HASTE sequence, two seemed to be explained by a signal cancelation defect within hepatic vessels. Indeed, both reviewers noted that in using the DL HASTE sequence, the intravascular signal was not canceled in some slices, particularly in the hepatic veins. These focal intravascular hypersignals could therefore potentially induce the detection of false-positives, especially when they are localized in only one slice. This artifact is identifiable, especially on large- and medium-caliber vessels, because it follows a vascular pathway and the hypersignal takes on a long form or dichotomous appearance (Fig. 4). In addition, the analysis of the overlying and underlying slices allows tracking of the vessel and confirming that the artifact is intravascular.

No explanation was found regarding the last of the three false-positives for the DL HASTE sequence. The five true-positives visible only on the T2-weighted BLADE sequence seemed to be explained by the absence of slice passing through these small lesions on the DL HASTE sequence. This could be explained by a bad breath-hold of the patient.

In a study in abdominal MRI at 1.5 T [22], Herrmann et al noted, in contrast to our study, a better image quality and diagnostic confidence of the T2-weighted BLADE sequence compared to the DL HASTE sequence. We used a higher magnetic field (3 T) to increase the signal-to-noise ratio and possibly the spatial resolution. The neural network of the DL HASTE sequence used in the 1.5-T MRI is different from the one at 3 T to increase denoising while also increasing blur. In addition, the spatial resolution was increased as a result of the larger matrix size we used.

Similarly, in the study by Mulé et al [23], the DL HASTE and T2-weighted BLADE sequences were compared for liver

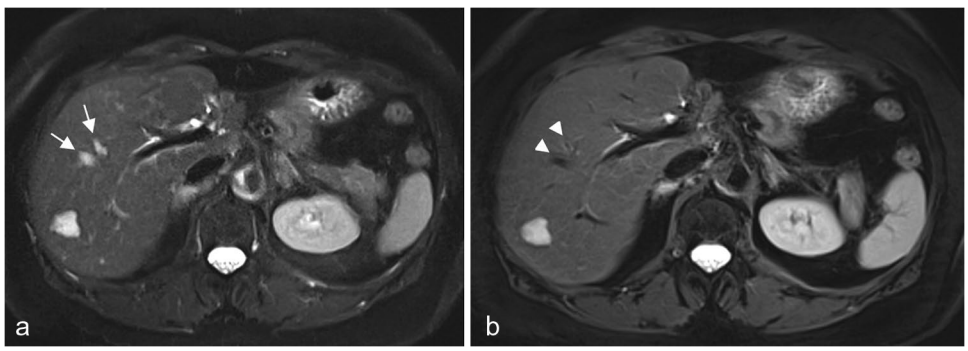

Fig. 4 Postoperative control of a left liver lobectomy for angiomyolipoma in a 70-year-old female. The DL HASTE axial image (**a**) shows two focal hypersignals mimicking liver lesions (arrows) corresponding to an uncanceled intravascular signal from the hepatic veins. Those hypersignals are not visible on the axial T2-weighted BLADE image (arrowheads) (**b**)

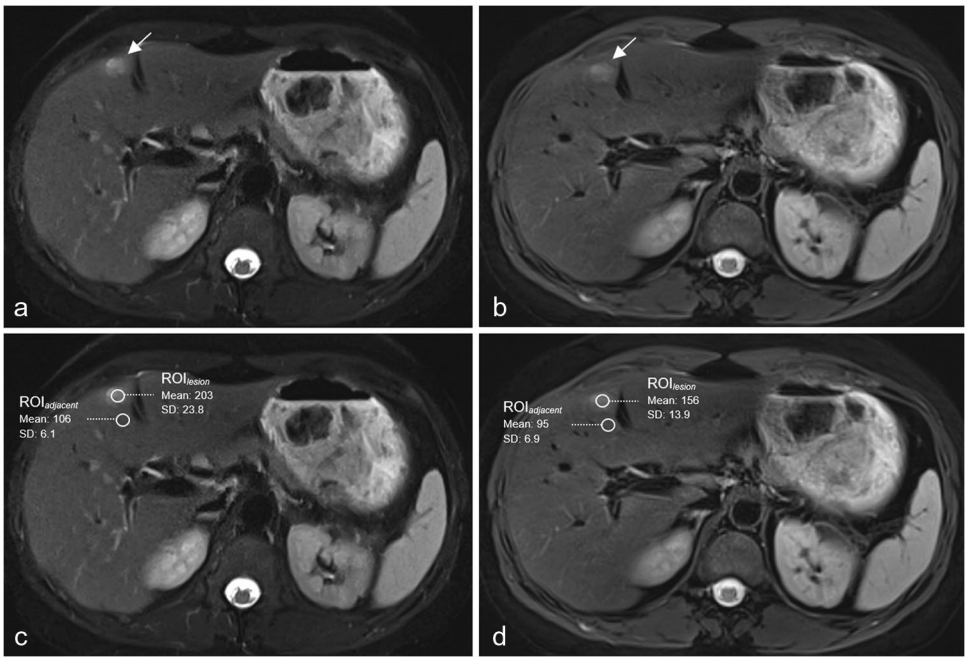

Fig. 5 Characterization of focal liver lesions in a 38-year-old female followed for adrenocortical cancer. The DL HASTE axial image (**a**) shows better conspicuity of a segment IV liver lesion (arrow) than the T2-weighted BLADE axial image (**b**). Two identical regions of interest (ROIs) are placed within the lesion (ROI_{lesion}) and in adjacent healthy liver ($ROI_{adjacent}$) on the HASTE DL image (**c**). The values indicate the mean and standard deviation of the signal. **d** The procedure is repeated identically on the T2-weighted BLADE image. We found a higher lesion contrast-to-noise ratio (CNR) on the HASTE DL image (CNR, 15.9) than on the T2-weighted BLADE image (CNR, 8.8), based on the previously described calculation method

MRI at 1.5 T. Similar to our study, their results showed a better image quality and a better CNR using the DL HASTE sequence. Contrary to our results, the SNR was better using the DL HASTE sequence. A possible explanation could be the different calculation methods between our two studies.

Shanbhogue et al [24] also noted an improved overall image quality, a reduction in the presence of artifacts, and an improved lesion visibility using the DL HASTE sequence. This study compares the DL HASTE sequence with the conventional turbo spin echo sequence without the technique of oversampling the data bands in a rotational manner around the center of the k-space (PROPELLER technique), which improves the image quality and reduces the presence of artifacts. As previously described, this study used a lower magnetic field (1.5 T) and a smaller matrix size.

Another study compared the DL HASTE sequence with two different flip angle evolution patterns to the T2-weighted BLADE sequence for abdominal MRI at 3 T [25]. Contrary to our study, these authors noted a better quality, sharpness, and contrast and less noise when using the T2-weighted BLADE sequence than using the DL HASTE sequence. A possible explanation may be the larger matrix and longer TE of the DL HASTE sequence used in our study, which could

Table 5 Results of the complementary analysis of the DL HASTE and T2-weighted BLADE sequences

Variables	DL HASTE		T2-weighted BLADE	
Total number of supernumerary lesions, *n*	41		5	
	TP	FP	TP	FP
Number of lesions, *n* (%)	38 (93)	3 (7)	5 (100)	0 (0)
Size of lesion, mm				
Median	6,5	6	6	/
IQR	5;7	5,5;7	5;7	/
Location of lesions, segments, *n* (%)				
1	1 (2)	0 (0)	0 (0)	/
2	11 (27)	0 (0)	1 (20)	/
3	5 (12)	0 (0)	0 (0)	/
4	4 (10)	0 (0)	1 (20)	/
5	2 (5)	0 (0)	2 (40)	/
6	4 (10)	2 (67)	1 (20)	/
7	5 (12)	1 (33)	0 (0)	/
8	9 (22)	0 (0)	0 (0)	/

Abbreviations: *DL HASTE*, half-Fourier acquisition single-shot turbo spin echo using deep learning; *IQR*, interquartile range; *TP*, true-positives; *FP*, false-positives

improve the spatial resolution and T2 contrast. Conversely, the matrix size of our T2-weighted BLADE sequence was smaller than in that in their study.

More recently, Ginocchio et al found similar results to our study for liver MRI at 3 T for overall quality, artifact reduction, lesion conspicuity, and lesion detection for the DL HASTE sequence [26]. This study included a small sample of participants in comparison with the conventional T2-weighted TSE sequence with potentially worse image quality and more artifacts than a sequence using a PROPELLER technique. The matrix size of both sequences was also smaller than in our study.

Several limitations in our study must be mentioned.

First, given its single-center design, our study may suffer from potential selection bias.

Second, since both sequences compared in our study are based on parallel imaging, the estimation of both SNR and CNR is difficult, and the technique implemented in our study corresponds to a local estimation close to the region of interest. This approach has the advantage of being fast and easy to perform. Only a noise measurement from a phantom or acquiring the same image twice would enable measuring the overall noise of the image [21, 36].

Concerning the greater number of focal hepatic lesions detected using the DL HASTE sequence, we recall that no histopathological confirmation has been performed on these supernumerary lesions detected only on the DL HASTE sequence despite a joint analysis of the other MRI sequences.

Contrary to a previous abdominal MRI study at 1.5 T, we did not compare the DL HASTE sequence with the conventional HASTE sequence because this sequence is not performed in liver MRI at our center as a part of clinical practice. This would have been an interesting avenue of research to study the neural network modifications on the conventional HASTE sequence, especially in pancreatic MRI or cholangio-MRI, where this sequence is used in routine practice.

In conclusion, our findings show that the DL HASTE sequence is more robust to artifacts, particularly motion artifacts, than the T2-weighted BLADE sequence. It also features better image quality and excellent contrast, allowing a greater number of hepatic lesions to be detected than with the T2-weighted BLADE sequence.

Supplementary Information The online version contains supplementary material available at https://doi.org/10.1007/s00330-023-09693-y.

Funding The authors state that this work has not received any funding.

Declarations

Guarantor The scientific guarantor of this publication is Valérie Laurent.

Conflict of interest Three authors of this manuscript declare relationships with the following companies: A.K., D.N., and S.A. are employees of Siemens Healthineers. These three authors were not involved in the acquisition or analysis of the data and did not have access to patient data. These three authors participated in the development of the DL HASTE sequence that was provided to us as part of a research project. The other authors of this manuscript declare no relationships with any companies, whose products or services may be related to the subject matter of the article.

Statistics and biometry One of the authors has significant statistical expertise.

Informed consent Written informed consent was obtained from all subjects (patients) in this study.

Ethical approval Institutional Review Board approval was obtained.

Methodology
- prospective
- observational
- performed at one institution

References

1. Choi SH, Kim SY, Park SH et al (2018) Diagnostic performance of CT, gadoxetate disodium-enhanced MRI, and PET/CT for the diagnosis of colorectal liver metastasis: systematic review and meta-analysis. J Magn Reson Imaging 47:1237–1250
2. Kim SY, An J, Lim Y-S et al (2017) MRI with liver-specific contrast for surveillance of patients with cirrhosis at high risk of hepatocellular carcinoma. JAMA Oncol 3:456–463
3. Schima W, Kölblinger C, Ba-Ssalamah A (2012) Non-invasive diagnosis of focal liver lesions: an individualized approach. Cancer Imaging 12:365–372
4. Hwang J, Kim SH, Lee MW, Lee JY (2012) Small (≤ 2 cm) hepatocellular carcinoma in patients with chronic liver disease: comparison of gadoxetic acid-enhanced 3.0 T MRI and multiphasic 64-multirow detector CT. Br J Radiol 85:e314-322
5. Augui J, Vignaux O, Argaud C, Coste J, Gouya H, Legmann P (2002) Liver: T2-weighted MR imaging with breath-hold fast-recovery optimized fast spin-echo compared with breath-hold half-Fourier and non–breath-hold respiratory-triggered fast spin-echo pulse sequences. Radiology 223:853–859
6. Lee SS, Byun JH, Hong H-S et al (2007) Image quality and focal lesion detection on T2-weighted MR imaging of the liver: comparison of two high-resolution free-breathing imaging techniques with two breath-hold imaging techniques. J Magn Reson Imaging 26:323–330
7. Serai SD, Hu HH, Ahmad R et al (2020) Newly developed methods for reducing motion artifacts in pediatric abdominal MRI: tips and pearls. AJR Am J Roentgenol 214:1042–1053
8. Dohan A, Gavini J-P, Placé V et al (2013) T2-weighted MR imaging of the liver: qualitative and quantitative comparison of SPACE MR imaging with turbo spin-echo MR imaging. Eur J Radiol 82:e655-661
9. Shaikh J, Stoddard PB, Levine EG et al (2019) View-sharing artifact reduction with retrospective compressed sensing reconstruction in the context of contrast-enhanced liver MRI for hepatocellular carcinoma (HCC) screening. J Magn Reson Imaging 49:984–993
10. Yoon JK, Kim M-J, Lee S (2019) Compressed sensing and parallel imaging for double hepatic arterial phase acquisition in

gadoxetate-enhanced dynamic liver magnetic resonance imaging. Invest Radiol 54:374–382
11. Rosenkrantz AB, Mannelli L, Mossa D, Babb JS (2011) Breath-hold T2-weighted MRI of the liver at 3T using the BLADE technique: impact upon image quality and lesion detection. Clin Radiol 66:426–433
12. Zhang L, Tian C, Wang P et al (2015) Comparative study of image quality between axial T2-weighted BLADE and turbo spin-echo MRI of the upper abdomen on 3.0 T. Jpn J Radiol 33:585–590
13. Kim BS, Kim JH, Choi GM et al (2008) Comparison of three free-breathing T2-weighted MRI sequences in the evaluation of focal liver lesions. AJR Am J Roentgenol 190:W19-27
14. Hirokawa Y, Isoda H, Maetani YS, Arizono S, Shimada K, Togashi K (2008) MRI artifact reduction and quality improvement in the upper abdomen with PROPELLER and prospective acquisition correction (PACE) technique. AJR Am J Roentgenol 191:1154–1158
15. Kang KA, Kim YK, Kim E et al (2015) T2-weighted liver MRI using the MultiVane technique at 3T: comparison with conventional T2-weighted MRI. Korean J Radiol 16:1038–1046
16. Nanko S, Oshima H, Watanabe T, Sasaki S, Hara M, Shibamoto Y (2009) Usefulness of the application of the BLADE technique to reduce motion artifacts on navigation-triggered prospective acquisition correction (PACE) T2-weighted MRI (T2WI) of the liver. J Magn Reson Imaging 30:321–326
17. Canellas R, Rosenkrantz AB, Taouli B et al (2019) Abbreviated MRI protocols for the abdomen. Radiographics 39:744–758
18. Marks RM, Ryan A, Heba ER et al (2015) Diagnostic per-patient accuracy of an abbreviated hepatobiliary phase gadoxetic acid-enhanced MRI for hepatocellular carcinoma surveillance. AJR Am J Roentgenol 204:527–535
19. Guglielmo FF, Mitchell DG, Roth CG, Deshmukh S (2014) Hepatic MR imaging techniques, optimization, and artifacts. Magn Reson Imaging Clin N Am 22:263–282
20. Donato H, França M, Candelária I, Caseiro-Alves F (2017) Liver MRI: from basic protocol to advanced techniques. Eur J Radiol 93:30–39
21. Schoenberg SO, Dietrich O, Reiser MF (2007) Parallel imaging in clinical MR applications, 1st edn. Springer, Berlin, Heidelberg, New York
22. Herrmann J, Gassenmaier S, Nickel D et al (2021) Diagnostic confidence and feasibility of a deep learning accelerated HASTE sequence of the abdomen in a single breath-hold. Invest Radiol 56:313–319
23. Mulé S, Kharrat R, Zerbib P et al (2022) Fast T2-weighted liver MRI: image quality and solid focal lesions conspicuity using a deep learning accelerated single breath-hold HASTE fat-suppressed sequence. Diagn Interv Imaging 103:479–485
24. Shanbhogue K, Tong A, Smereka P et al (2021) Accelerated single-shot T2-weighted fat-suppressed (FS) MRI of the liver with deep learning-based image reconstruction: qualitative and quantitative comparison of image quality with conventional T2-weighted FS sequence. Eur Radiol 31:8447–8457
25. Herrmann J, Nickel D, Mugler JP et al (2021) Development and evaluation of deep learning-accelerated single-breath-hold abdominal HASTE at 3 T using variable refocusing flip angles. Invest Radiol 56:645–652
26. Ginocchio LA, Smereka PN, Tong A et al (2023) Accelerated T2-weighted MRI of the liver at 3 T using a single-shot technique with deep learning-based image reconstruction: impact on the image quality and lesion detection. Abdom Radiol (NY) 48:282–290
27. Loening AM, Saranathan M, Ruangwattanapaisarn N, Litwiller DV, Shimakawa A, Vasanawala SS (2015) Increased speed and image quality in single-shot fast spin echo imaging via variable refocusing flip angles. J Magn Reson Imaging 42:1747–1758
28. Hammernik K, Klatzer T, Kobler E et al (2018) Learning a variational network for reconstruction of accelerated MRI data. Magn Reson Med 79:3055–3071
29. Nesterov Y (1983) A method for solving the convex programming problem with convergence rate O(1/k^2). Dokl Akad Nauk SSSR 269:543–547
30. Jégou S, Drozdzal M, Vazquez D, Romero A, Bengio Y (2017) The one hundred layers tiramisu: fully convolutional DenseNets for semantic segmentation. IEEE conference on computer vision and pattern recognition workshops (CVPRW). https://doi.org/10.1109/CVPRW.2017.156
31. Soyer P (1993) Segmental anatomy of the liver: utility of a nomenclature accepted worldwide. Am J Roentgenol 161:572–573
32. Dietrich O, Raya JG, Reeder SB, Ingrisch M, Reiser MF, Schoenberg SO (2008) Influence of multichannel combination, parallel imaging and other reconstruction techniques on MRI noise characteristics. Magn Reson Imaging 26:754–762
33. Heverhagen JT (2007) Noise measurement and estimation in MR imaging experiments. Radiology 245:638–639
34. Zhang Z, Gayle AA, Wang J, Zhang H, Cardinal-Fernández P (2017) Comparing baseline characteristics between groups: an introduction to the CBCgrps package. Ann Transl Med 5:484
35. Gerard E. B, Mary A, Jennie C (2006) An interactive taxonomy of MR imaging sequences. Radiographics 26:e24; quiz e24
36. Dietrich O, Raya JG, Reeder SB, Reiser MF, Schoenberg SO (2007) Measurement of signal-to-noise ratios in MR images: influence of multichannel coils, parallel imaging, and reconstruction filters. J Magn Reson Imaging 26:375–385